

Statistically sound application of fiber push-out method for the study of locally non-uniform interfacial properties of SiC-SiC fiber composites

A. Hussey^a, R. De Meyere^a, C. Deck^b, D. E. J. Armstrong^a, Y. Zayachuk^{a,*}
^a*University of Oxford, Department of Materials, Parks Road, Oxford, OX1 3PH, UK*
^b*General Atomics, P.O. Box 85608, San Diego, CA, 92186-5608, USA*

*Corresponding author: yevhen.zayachuk@materials.ox.ac.uk; + 44 (0) 1865 283659.

Abstract

Push-out tests were performed on SiC-SiC fiber composites with single- and multi-layered pyrolytic carbon fiber-matrix interphases. It is shown that experimental scatter is significant and a large number of tests is necessary in order to obtain statistically relevant values of interfacial shear strength. A difference between different regions of an individual fiber tow is observed, linked to a local porosity. It is shown that interfacial debonding occurs along the boundary between the fiber and the first carbon layer, regardless of the structure of the interphase, and thus interfacial shear strength is not directly linked to the structure of the interphase.

Keywords

Ceramic matrix composites (CMC); interfaces; push-out testing.

Silicon carbide (SiC) attracts considerable interest as a candidate material for aerospace [1] and nuclear [2,3] applications due to its high temperature strength, creep resistance [4], oxidation resistance [5], and radiation tolerance [6]. In particular, it is considered for its use in aero-engines [7,8,9] and novel accident-tolerant core (ATC) and accident-tolerant fuel (ATF) concepts [10]. In order to overcome its inherent brittleness [11], while retaining beneficial chemical and nuclear properties, it is suggested to be used in the form of a continuous SiC fiber-reinforced SiC matrix (SiC-SiC) composite [12].

Pseudo-ductile behaviour is introduced via crack deflections and crack bridging, which occur at fiber-matrix interphase [13,14]. Therefore, the fracture properties of a composite are largely determined by the properties of its interphase, which needs to have low-toughness (promoting crack deflection), and high sliding friction coefficient (increasing energy absorption during fiber sliding) [15,16,17]. Various methods have been suggested for the characterization of these interphases, including micropillar compression [18], microcantilever fracture [19], fiber pull-out [20,21] and fiber push-out [22]. These methods determine different interfacial parameters, but in terms of experimental methodology they can be divided into two major groups – the ones that require manufacturing of each individual micro-specimen prior to testing (micropillar, microcantilever and pull-out testing) and the ones that allow for multiple tests on multiple fibers using a single prepared sample, thus potentially providing much higher number of tests and much better statistics (fiber push-out).

Push-out is a well-established method for measuring the interfacial properties. In this method, a thin sample (typically in the range of 50 – 100 μm) is manufactured in which the fibers are running in the direction as close to normal to the surface as possible. Load is applied to an individual fiber using a nanoindenter, until debonding occurs and the fiber is displaced. The technique provides the values of interfacial shear strength (ISS) and interfacial sliding friction coefficient.

Push-out testing is conceptually a rather simple technique. However, a review of the available literature indicates that there exist several common issues with it. Firstly, the reported tests are rarely done to a statistically meaningful level, with only a few tests being typically performed (low dozens, or as few as one or two [23]) due to the technical difficulties associated with manufacturing and handling of the sufficiently thin samples. Secondly, the microstructure is usually not taken into account in the analysis of these measurements, despite composite microstructure being very non-uniform. Lastly, in many reported studies, a sharp indenter tip (e.g. Berkovich) is used [24,25,26]. This causes extensive plastic deformation, and even cracking, of the fibre before the debonding can occur, which changes the shape of the fibre and load distribution, thus modifying results.

The presented study focused on two issues: (1) comparison of different parts of fiber tows – observing the variability of the ISS with local environment surrounding an individual fiber, which varies within a tow; (2) comparison of different composite grades with different structures of the interphase.

In order to obtain reliable measurement statistics, a large number of tests – on the order of a hundred – was performed, yielding statistically sound results on interfacial shear strength (ISS). In order to avoid plastic deformation of the fiber during loading, a flat punch tip was used. As evidenced by Fig. 1a, while it is possible to see the impression left in the fiber material by the tip, the resulting plastic deformation is minor. Finally, the influence of the local microstructure – namely, degree of porosity in the vicinity of each individual fiber, as determined by scanning electron microscopy (SEM) imaging – was taken into account.

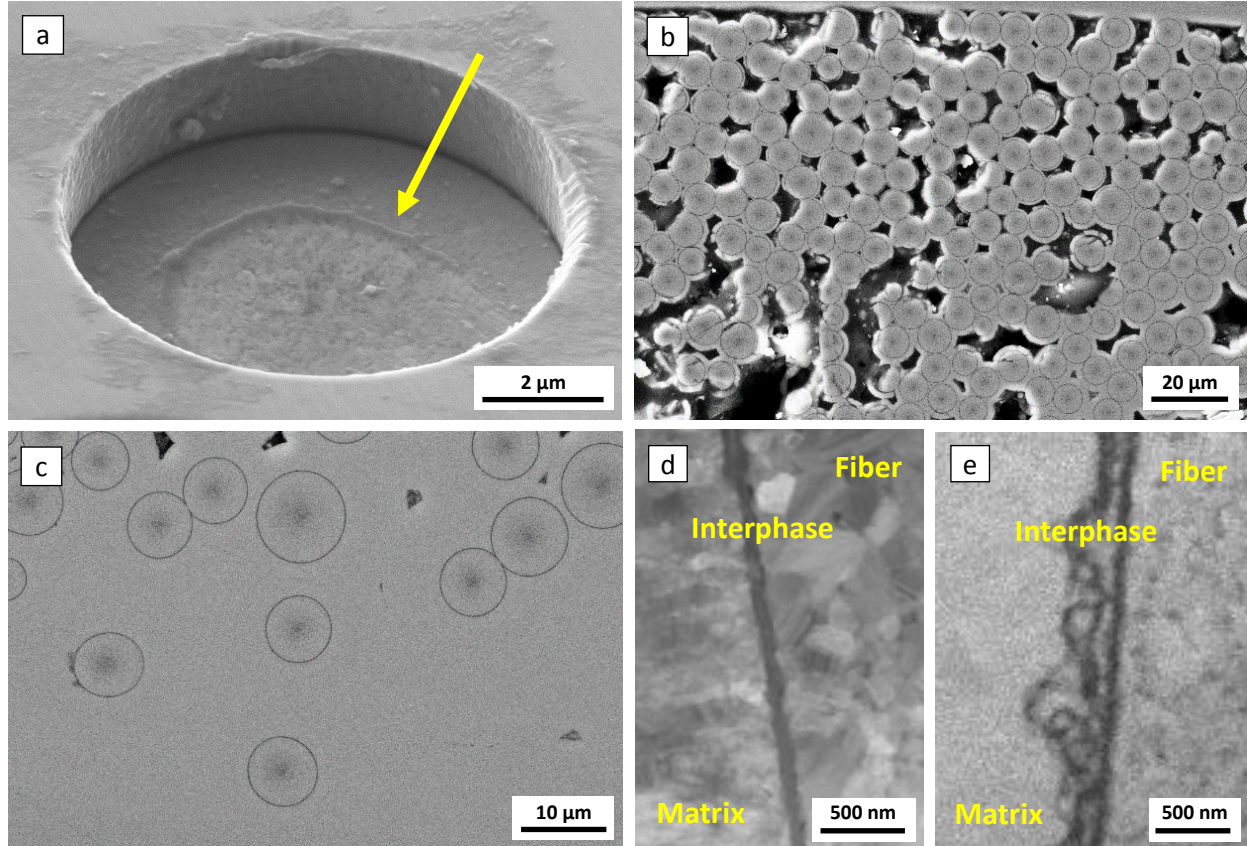


Fig. 1 (a) An image of the impression left by a flat-punch tip on the fiber (indicated by an arrow), indicating minor plastic deformation during loading; (b) highly porous central part of a typical fiber tow; (c) relatively monolithic periphery of a typical fiber tow; (d) STEM image of a single-layered interphase; PyC layer is visible as a dark band; (e) STEM image of a multi-layered interphase; PyC layers are visible as the dark bands, with bright regions between them correspond to an extra layer of SiC.

The relevance of the first problem – the difference of interfacial properties within a tow – is due to the composite growth method. The fiber composite considered in this study is formed by growing the SiC matrix onto a SiC fiber reinforcement structure [27]. While various methods are employed for this, depending on application, chemical vapour infiltration (CVI) is a preferable growth method specifically for nuclear applications, since it produces very high purity β -phase SiC with good radiation resistance [28]. The use of CVI leads to a significant multi-level porosity in the resulting material, with large pores between fiber tows, as well as much smaller pores between the individual fibers within a single tow [29].

The composite material used in this study was manufactured by General Atomics, using the CVI method with a reinforcement made of commercially available Tyranno SA3 fibers in a plain weave architecture. 1 presents the

comparison between the parts of an individual tow, showing the highly porous central part of a tow, where the majority of the fibers is in contact with a pore or another fiber, and the relatively monolithic periphery, where each fiber is well embedded in a uniform layer of matrix material.

The work on optimization of the properties of the composites is ongoing; in particular, an issue of the optimal structure of the interphase is being considered [30]. In this context, a composite grade with an interphase consisting of a single PyC layer was compared in this study to a grade with a multi-layered interphase, consisting of two PyC layers with an additional SiC layer in between them; Fig. 1 presents the scanning transmission electron microscopy (STEM) images (obtained using a JEOL JEM-2100 TEM) comparing the structures of the interphases of the two grades.

Experiments described here used an Agilent XP nanoindenter and a flat-punch indenter tip with a diameter of $\sim 5.4 \mu\text{m}$, i.e. smaller than the typical diameter of the fibers ($\sim 8 \mu\text{m}$). The nanoindenter is equipped with an x40 optical objective, able to resolve individual fibers; it was thus possible to precisely position the indenter tip and apply a load to an individual fiber. Fig. 2a and 2b present a collection of the experimental load-displacement curves, obtained in a number of successful push-out tests (i.e. the ones where the displacement of a fiber was confirmed) on a single-layered grade. An image of a pushed-out fiber is presented in Fig. 2c as an example of a successful test. The overall difference between the center (Fig. 2a) and the periphery (Fig. 2b) of the tows is noticeable, however, large scatter within each dataset is evident as well.

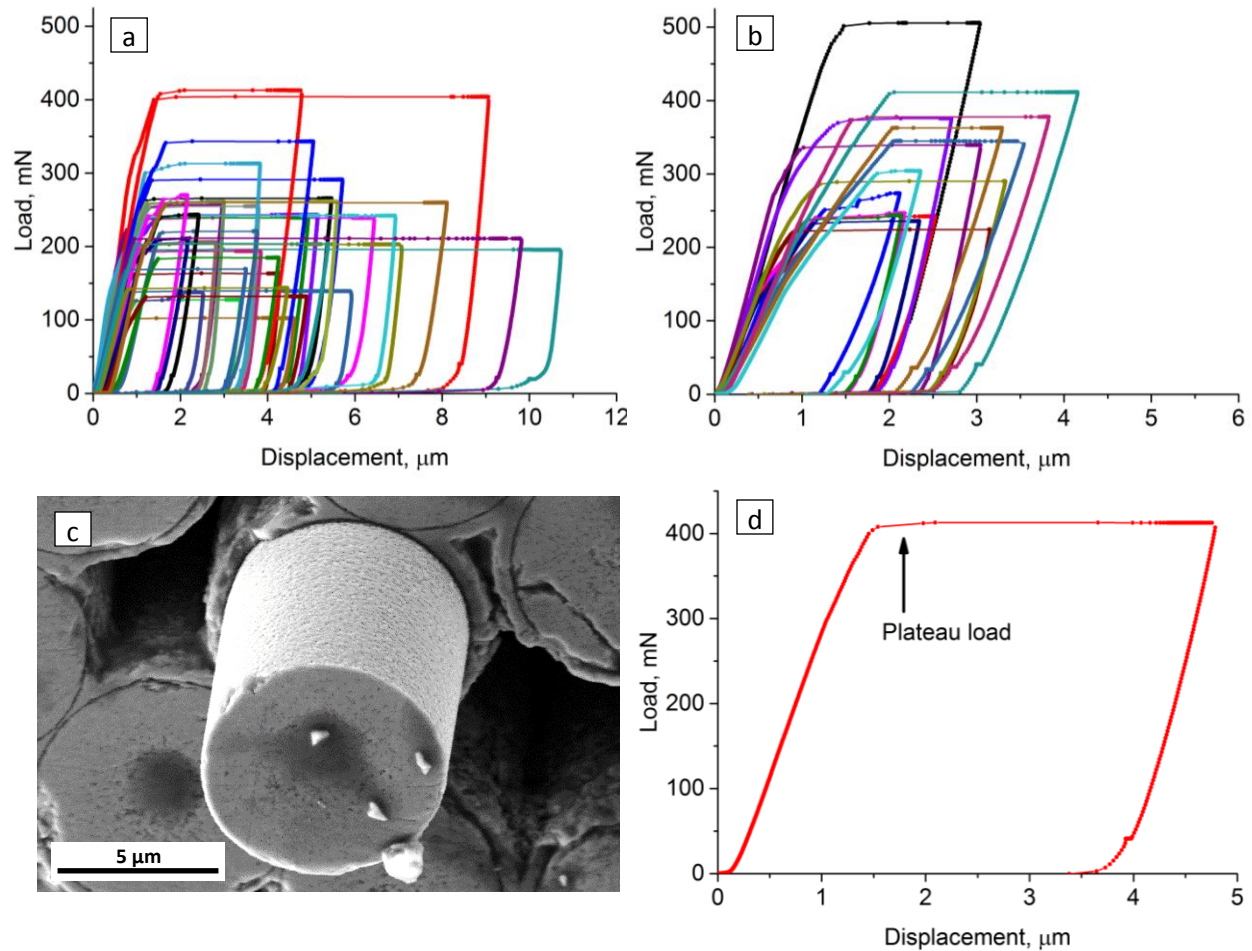


Fig. 2 (a) Results of the push-out tests in the center of the tows; (b) push-out tests at the periphery of the tows; (c) SEM image of a single fiber after successful push-out; (d) typical shape of a load-displacement curve.

Load-displacement curves (Fig. 2d) were analysed using a simple stress model, as described in [31,32], where the interfacial shear strength is calculated from the equation

$$\tau = \frac{F}{2\pi RH} \quad (\text{Equation 1})$$

where τ is the ISS, F is the plateau load (i.e., debonding load), R is the fibre radius and H is the sample thickness.

Resulting values of ISS for the single layer sample are presented in the Table 1. They were calculated to be 69.44 ± 21.9 MPa in the central part and 119.1 ± 19.7 MPa at the periphery of a tow. This correlates well with the distribution of internal porosity as imaged in the micrographs. Due to higher porosity the fibers in the center of a tow are less well bonded, and therefore the load needed to initiate interfacial debonding and to displace a fiber is lower. However, this observation suggests that an “effective ISS” should be defined for a fiber, and this will be different depending on where within a tow a particular fiber is located. This will take into account both the true strength of interfacial bonding, as well as the influence of the local environment surrounding this particular fiber.

Values of ISS measured for peripheral fibers can be considered to be close to the “true” ISS, i.e. a value determined exclusively by the properties of the interphase, since the effects of the environment can be excluded. On the other hand, the knowledge of the distribution of the effective ISS within a tow might be useful for rationalization of the macroscopic mechanical properties based on fundamental material parameters, since it allows a realistic description of the non-uniformity of the properties of fiber tows.

Table 1 Measured values of ISS and corresponding errors.

	Single-layered, MPa	Single-layered error, MPa	Multi-layered, MPa	Multi-layered error, MPa
Center	69.44	14.04	57.73	11.67
Periphery	119.1	24.07	89.72	18.14

Distribution of porosity within a fiber tow is similar in the multi-layered grade. Calculated values of ISS for this grade were 57.73 ± 16.60 MPa in the center 89.72 ± 16.40 MPa at the periphery. Comparison with the values obtained for a single-layered interphase grade indicates that the multi-layered ISS is somewhat lower. Since the peripheral values were established to be more representative of a true ISS, push-outs on the multi-layered grade indicate ~24% decrease in it (from 119 to 90 MPa).

The measured values of ISS show significant scatter, and it is necessary to discuss the sources of errors. Some errors were readily quantified, whilst others lent themselves more readily to qualitative analysis.

The quantifiable errors considered were those used in Equation 1: fibre radius R , push-out load F and fibre thickness H . The error in the diameter was entirely due to the error in reading the diameter from the images, the push-out load errors were due to systematic errors in the nanoindenter and the errors in thickness were due to the error in matching the thickness to the push-out area as well as reading the measurement from the image. Predominant contribution among these comes from the error in thickness. The only way to measure the thickness is to image the side of the sample. Under this orientation, it is impossible to see the push-out tests, so there is an element of uncertainty of where the pushed-out fibres are located. As the samples were not completely flat, this leads to a potentially large error, and thus 3 measurements of width were taken and averaged. The accuracy in measuring the radius was to the nearest 0.1 microns on each side of the fibre. The error in the load was estimated from the nanoindenter specifications. The approximate raw values, given in Table 2, are estimates of the mean value for each measurement.

Table 2 Uncertainties in the push-out measurements.

	Approximate raw error	Approximate raw value	Approximate percentage error
Radius (R)	0.1 μm	3.5 μm	2.9%
Load (F)	1 mN	250 mN	0.4%
Thickness (t)	15 μm	150 μm - 75 μm	10% - 20%

Therefore, the error in the interfacial shear strength follows the equation:

$$\delta\tau = \tau \left[\left(\frac{\delta R}{R} \right)^2 + \left(\frac{\delta F}{F} \right)^2 + \left(\frac{\delta t}{t} \right)^2 \right]^{\frac{1}{2}} \quad (\text{Equation 2})$$

Errors thus calculated are presented in the Table 1. Note that the errors for both the central regions is smaller than the standard deviation in the results. This is because the standard deviation results not only from the measurement uncertainty, but also represents the differing environments surrounding the fibers.

The errors that are not quantifiable are related to the direction of the fibre under the surface and potential relaxation of the matrix (where the hole in the matrix that constrains the fibre shrinks after push-out). It is assumed in Equation 4 that the fibres run perfectly perpendicular to the surface. This leads to errors with defining a peripheral fibre (the definition is based on the environment of the fibre, which could change under the surface of the sample as the fibres are not necessarily straight); breaking the assumptions of the equation (one of the key assumptions in the model is that the fibres run perpendicular to the surface from top to bottom); the uncertainty of the projection of the force (it is assumed that the angle between the surface and the fibre is 90°). The first of these points will lead to a slight underestimation of peripheral interfacial shear strength, as some fibres that appear to be peripheral may have environments more similar to central fibers under the surface. The second and third points lead to an overestimation of all interfacial shear strengths.

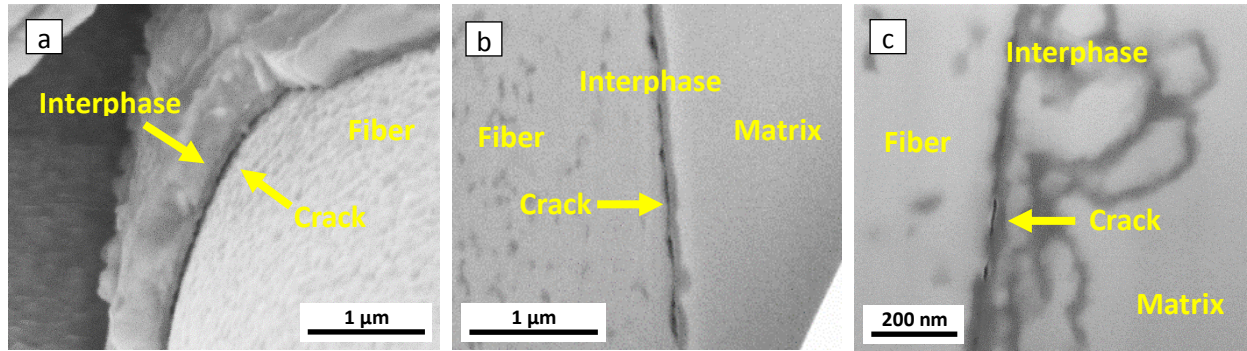


Fig. 3(a) Surface image of the near-interphase region in a single-layered grade sample following a push-out, showing debonding; (b) cross-section of the near-interphase region in a single-layered grade sample following a push-out, showing a crack path; (c) cross-section of the near-interphase region in a multi-layered grade sample following a push-out, showing a crack path.

Following push-out experiments, debonding was investigated using SEM. Fig. 3a shows a near-interphase region of a typical fiber in the single-layered grade following its push-out. Interphase can be seen as a dark stripe surrounding the pushed-out fiber, and it is evident that the crack is following the fiber-interphase boundary. In addition, the surfaces of the samples were cross-sectioned using focused ion beam in ZEISS Auriga dual-beam FEG SEM-FIB workstation, so that the resulting cross-sections contained the near-interphase regions, allowing imaging of the crack path in the vicinity of the interlayer. Fig. 3b shows an example of such cross-section of a typical push-out in the single-layered grade. Debonding can be observed, and it is seen the visible crack follows the fiber-interlayer boundary, in accordance to what is seen on the surface. This is similar to the character of interfacial debonding observed in the microcantilever tests in SiC-SiC with PyC interphase [19].

Fig. 3c presents an image of a cross-section of the near-interphase region of a multi-layered grade after the push-out. The crack path is visible – it is following the fiber-interlayer boundary, and as a result, it appears that only the first layer of the multi-layered structure is involved in the debonding and subsequent friction. No debonding occurring within the interphase, for example at the boundaries between individual layers, was observed. This is

similar to the behaviour of the multi-layered interphase of SiC-SiC composite produced using polymer infiltration and pyrolysis (PIP) method with KD-I fiber reinforcement, reported in [26].

The measured difference in ISS between single- and multi-layered grades is therefore not because of the difference in the character of crack propagation. It can thus be suggested that the ISS of an interphase is not a fundamental property of the interphase's internal structure, but is determined exclusively by the character of bonding between the SiC fiber and deposited PyC layer – which ultimately is determined by the details of a specifically implemented deposition process.

To summarize, presented data indicate that there is indeed large scatter in the values of ISS, measured using the push-out method. Therefore, in order to get statistically relevant data it is imperative to perform a large number of tests. Flat-punch tip is shown to be a requirement as well, since it has been shown to cause only a minor deformation of a fiber. Furthermore, there is a clear difference between different parts of a tow, which is linked to the difference in local environment, such as porosity. This environment is non-uniform within the tow, and as a consequence the measured ISS is lowest close to the tow core, where porosity is highest, and increases towards the periphery, where porosity is correspondingly lowest or non-existent. This suggests the introduction of a concept of “effective ISS”, which differs depending on fibre location within an individual tow. Knowledge of this is useful for understanding the behaviour of a composite as a whole; however, for characterization of specifically the interfacial bonding, true ISS is a relevant parameter and can be determined at the periphery of the tows, where the influence of porosity and other fibers is minimal or non-existent.

Comparison of the grades with different structures of the PyC interphases – single- and multi-layered – indicates that there is no difference in the character of crack propagation. Debonding occurs along the boundary between a SiC fiber and first layer of PyC, regardless of the interfacial structure. At the same time there is a difference in measured values of ISS. This leads to the suggestion that for a given kind of fiber the ISS is determined by the interfacial deposition process.

Acknowledgements

Funding: This work was supported by the EPSRC [grant number EP/N017110/1]. D. Armstrong acknowledges support from the Royal Academy of Engineering in the form of a Research Fellowship. This work was also supported by the U.S. Department of Energy (DOE), Office of Nuclear Energy's Nuclear Science User Facilities (NSUF) program and the DOE-NEUP program 15-8439.

References

- [1] J.A. DiCarlo, in: N.P. Bansal, J. Lamon (Eds.), *Advances in SiC/SiC Composites for Aero-Propulsion in Ceramic Matrix Composites: Materials, Modelling and Technology*, John Wiley & Sons, 2015.
- [2] K. Yueh, D. Carpenter, H. Feinroth, *Nuclear Engineering International* 55 (2010), 75-87.
- [3] X. Zhou, S. Zhao, P. Mummery, J. Marrow, *Key Engineering Materials* 602-603 (2014), 416-421.
- [4] C.H. Carter Jr., R.F. Davis, J. Bentley, *Journal of American Ceramic Society* 67 (1984) 732–740.
- [5] E.A. Gulbransen, S.A. Jansson, *Oxidation of Metlas* 4 (1972) 181–201.
- [6] R.J. Price, *Nuclear Technology* 35 (1977) 320–336.
- [7] G. Gardiner, *Aeroengine Composites, Part I: the CMC Invasion*, 2015. *Composites World*.
- [8] M. Fellet, *Ceramic-matrix composites take the heat*, *MRS Bulletin* 40 (2015).
- [9] F.W. Zok, *Ceramic-matrix composites enable revolutionary gains in turbine engine efficiency*, *Am. Ceram. Soc. Bull.* 95 (2016).
- [10] S.J. Zinkle, K.A. Terrani, J.C. Gehin, L.J. Ott, L.L. Snead, *Journal of Nuclear Materials* 448 (2014) 374-379.
- [11] H. Kikuchi, R.K. Kalia, A. Nakano, P. Vashishta, P.S. Branicio, F. Shimojo, *Journal of Applied Physics* 98 (2005) 103524.
- [12] S. Yajima, J. Hayashi, *Nature* 261 (1976) 683–685.
- [13] R. J. Kerans, R. S. Hay, T. A. Parthasarathy and M. K. Cinibulk, *Interface Design for Oxidation-Resistant Ceramic Composites*, *Journal of American Ceramic Society* 85 (2002) 2599–2632.
- [14] X. W. Yin, L. F. Cheng, L. T. Zhang, N. Travitzky and P. Greil, *Fibre-reinforced multifunctional SiC matrix composite materials*, *International Materials Reviews* 62 (2017) 117–172.
- [15] J.K. Wells and P.W.R. Beaumont, *Crack-tip energy absorption processes in fibre composites*, *Journal of Materials Science* 20 (1985) 2735-2749.
- [16] D. Hull, *An introduction to composite materials*, Cambridge University Press (1992).

- [17] B.F. Sorensen and R. Talreja, Analysis of Damage in a Ceramic Matrix Composite, *International Journal of Damage Mechanics* 2 (1993) 246–271.
- [18] J. Kabel, P. Hosemann, Y. Zayachuk, D. E. J. Armstrong, T. Koyanagi, Y. Katoh, and C. Deck, Ceramic composites: A review of toughening mechanisms and demonstration of micropillar compression for interface property extraction, *Journal of Materials Research* 33 (2018), 424–439.
- [19] Y. Zayachuk, P. Karamched, C. Deck, P. Hosemann, and D. E.J. Armstrong, *Acta Materialia* 168 (2019) 178–189.
- [20] G.A. Cooper, The Fracture Toughness of Composites Reinforced with Weakened Fibers, *Journal of Materials Science* 5 (1970) 645–654.
- [21] Interfacial Debonding and Fiber Pull-out Stresses of Fiber-reinforced Composites II: Non-constant Interfacial Bond Strength, *Materials Science and Engineering*, A125 (1990) 67–73.
- [22] J.D. Bright, D.K. Shetty, C.W. Griffin, and S.Y. Limaye, Interfacial Bonding and Friction in Silicon Carbide (Filament)-Reinforced Ceramic- and Glass-Matrix Composites, *Journal of American Ceramic Society* 72 (1989) 1891–1898.
- [23] F. Rebillat, J. Lamon, and A. Guette, Concept of a strong interface applied to SiC/SiC composites with a BN interphase, *Acta Materialia* 48 (2000) 4609–4618.
- [24] T. Nozawa, Y. Katoh, and L.L. Snead, The effect of neutron irradiation on the fiber/matrix interphase of silicon carbide composites, *Journal of Nuclear Materials* 384 (2009) 195–211.
- [25] W.M. Mueller, J. Moosburger-Will, M.G.R. Sause, S. Horn, Microscopic analysis of single-fiber push-out tests on ceramic matrix composites performed with Berkovich and flat-end indenter and evaluation of interfacial fracture toughness, *Journal of the European Ceramic Society* 33 (2013) 441–451.
- [26] H. Yu, X. Zhou, W. Zhang, H. Peng, C. Zhang, Mechanical behavior of SiCf/SiC composites with alternating PyC/SiC multilayer interphases, *Materials and Design* 44 (2013) 320–324.
- [27] L.L. Snead, T. Nozawa, Y. Katoh, T.S. Byun, S. Kondo, D.A. Petti, *Journal of Nuclear Materials* 371 (2007) 329–377.
- [28] M.E. Sawan, N.M. Ghoniem, L. Snead, Y. Katoh, *Journal of Nuclear Materials*, 417 (2011) 445–450.
- [29] C.P. Deck, H.E. Khalifa, B. Sammulu, T. Hilsabeck, C.A. Back, Fabrication of SiC-SiC composites for fuel cladding in advanced reactor designs, *Progress in Nuclear Energy* 57 (2012) 38–45.
- [30] H.J. Yu, X.G. Zhou, W. Zhang, H.X. Peng, C.R. Zhang, Z.L. Huang, Mechanical properties of 3D KD-I SiCf/SiC composites with engineered fibre-matrix interfaces, *Composites Science and Technology* 71 (2011) 699–704.
- [31] W. Yang et al., *Journal of Nuclear Materials*, 307 (2002) 1088–1092.
- [32] H. J. Yu, X. G. Zhou, W. Zhang, H. X. Peng, C. R. Zhang, and Z. L. Huang, *Composites Science and Technology* 71 (2011) 699–704.